Clim Dyn
DOI 10.1007/s00382-008-0504-5

# Trends and variability of storminess in the Northeast Atlantic region, 1874–2007

Xiaolan L. Wang · Francis W. Zwiers ·
Val R. Swail · Yang Feng

Received: 4 July 2008 / Accepted: 28 November 2008


Abstract This article builds on the previous studies on storminess conditions in the northeast North Atlantic–European region. The period of surface pressure data analyzed is extended from 1881–1998 to 1874–2007. The seasonality and regional differences of storminess conditions in this region are also explored in more detail. The results show that storminess conditions in this region have undergone substantial decadal or longer time scale fluctuations, with considerable seasonal and regional differences. The most notable differences are seen between winter and summer, and between the North Sea area and other parts of the region. In particular, winter storminess shows an unprecedented maximum in the early 1990s in the North Sea area and a steady upward trend in the northeastern part of the region, while it appears to have declined in the western part of the region. In summer, storminess appears to have declined in most parts of this region. In the transition seasons, the storminess trend is characterized by increases in the northern part of the region and decreases in the southeastern part, with increases in the north being larger in spring. In particular, the results also show that the earliest storminess maximum occurred in summer (around 1880), while the latest storminess maximum occurred in winter (in the early 1990s). Looking at the annual metrics alone (as in previous studies), one would conclude that the latest storminess maximum is at about the same level as the earliest storminess maximum, without realizing that this is comparing the highest winter storminess level with the highest summer storminess level in the period of record analyzed, while winter and summer storminess conditions have undergone very different long-term variability and trends. Also, storminess conditions in the NE Atlantic region are found to be significantly correlated with the simultaneous NAO index in all seasons but autumn. The higher the NAO index, the rougher the NE Atlantic storminess conditions, especially in winter and spring.

X. L. Wang (✉) · F. W. Zwiers · V. R. Swail · Y. Feng
Climate Research Division, Atmospheric Science and Technology Branch, Environment Canada, 4905 Dufferin Street, Toronto, ON M3H 5T4, Canada
e-mail: Xiaolan.Wang@ec.gc.ca

## 1 Introduction

Recently, Gillett et al. (2003, 2005) analyzed mean sea level pressure (SLP) from 1948 to 2005 for DJF and found decreases in pressure over the Arctic, Antarctic and North Pacific, with increases over the subtropical North Atlantic, southern Europe and North Africa. Wang et al. (2008) analyzed geostrophic wind energy index (squared SLP gradients) derived from the same SLP data as in Gillett et al. (2005) and found that winter (JFM) geostrophic wind energy has increased over the high-latitude North Atlantic and North Pacific storm track regions, but decreased over the mid-latitude North Atlantic. Cyclone activity has changed in a consistent manner over the second half of the 20th century, with a significant decrease in the mid-latitudes and an increase in the high latitudes of the northern hemisphere, indicating a poleward shift of the storm track in winter (McCabe et al. 2001; Gulev et al. 2001; Wang et al. 2006a, b). Thus the observational evidence indicates that the strength of mid-latitude SLP gradients and associated westerly circulation has increased in the northern hemisphere, especially during winter, since at least the late 1970s (Trenberth et al. 2007).

Published online: 19 December 2008

Nevertheless, there are also contrasting studies which show that the recent maximum of storminess as measured by annual metrics in the northeast Atlantic sector is at about the same level of storminess as in the late 19th century (e.g., WASA 1998; Schmidt and von Storch 1993). In particular, analyzing geostrophic wind speeds calculated from in situ observations of surface pressure over the northeast Atlantic-European region for the period from 1881 up to 1998, Alexandersson et al. (1998, 2000) reported a decline of storminess from high levels during the late nineteenth century to a minimum around 1960 and then a quite rapid increase to a maximum around 1990, followed again by a slight decline at the end of the period analyzed. Recently, Matulla et al. (2008) reached a similar conclusion when they used the same approach and the pressure data for 1880-2005 to update one of the pressure triangles analyzed by Alexandersson et al. (1998, 2000). Alternatively, Schmith et al. (1998) analyzed the 50th, 90th and 99th percentiles of absolute 24-h pressure tendencies at eight stations in this region and reported similar characteristics of long-term variability of storminess. These long-term variability characteristics describe changes seen in the regional average series of annual high-percentiles of geostrophic wind speeds. The use of annual metrics and area average may, however, have masked evidence of changes in seasonality of storminess and spatial shifts in the storm track. Hence, there is a need to explore seasonal and regional differences, and also to update the studies of Alexandersson et al. (2000) with pressure data for the last 9 years (1999–2007). These needs motivate the present study. We have therefore analyzed in-situ surface pressure data for the period from January 1874 to January 2008 in order to update the studies of Alexandersson et al. (1998, 2000), and to explore seasonal and regional differences of storminess in more detail.

The remainder of this article is organized as follows. The data and processing procedures are described in Sect. 2. The results are presented and discussed in Sect. 3. The relationship of storminess conditions to the North Atlantic Oscillation (NAO) is explored in Sect. 4. This article is completed with a few concluding remarks in Sect. 5.

## 2 Data and procedure

The surface pressure observations analyzed in this study were taken from the Integrated Surface Pressure Databank (Gleason et al. 2008). The pre-1996 pressure data is part of a larger dataset published in Schmith et al. (1997). The stations providing the historical sea level pressure (SLP) data analyzed in this study are listed in Table 1. The period of record extends from January 1868 or later to January 2008, but the data from the Bergen site for the pre-1874 period were not used in this study because all the other sites have no data for this early period. Note that two station IDs that share the same first 5 digits (see Table 1) are actually the previous and current IDs of the same station; stations with 6-digit IDs (with the last digit being 0) are currently active stations. For clarity, hereafter, the word "station" is used to refer to a data record associated with a unique ID, while "site" is used to refer to the combination of two stations that are very close to each other (see Table 1). For example, the combination of stations 04013 and 040130, which have the same name and same lat/long (not shown), is referred to as site Sty (see Table 1). The single station site Pre is used only to fill in a data gap in the Abe site record (details given near the end of this section).

Table 1 The 11 sites and the related stations of sea level pressure (SLP) data analyzed in this study

| Site | Name of station(s) | Country | Station IDs | Period of data used (YYYY.MM.DD.HH) |
|---|---|---|---|---|
| Sty | Stykkisholmur | Iceland | 04013; 040130 | 1874.01.01.10–2008.01.03.21 |
| Bod | Bodoe; Bodo VI | Norway | 01152; 011520 | 1900.01.01.08–2008.01.03.23 |
| Tor | Torshavn | Faroe Islands | 06011; 060110 | 1874.01.01.09–2008.01.03.06 |
| Ber | Bergen-Fredriksberg; Bergen Flesland | Norway | 01316; 013110 | 1868.01.01.08–2008.01.03.23 |
| Abe | Aberdeen/Dyce Airport; Aberdeen Obs. | Great Britain | 03091; 030910 | 1871.01.01.07–2008.01.03.23 (no data for 1948–1956) |
| Pre | Prestwick(Civ/Navy) | Great Britain | 031350 | 1944.01.01.00–2002.07.10.18 |
| Val | Valentia Observatory; Valentia Obs. | Ireland | 03953; 039530 | 1892.01.01.09–2008.01.03.23 |
| Ves | Vestervig; Thyboroen | Denmark | 21100; 060520 | 1874.01.01.08–2008.01.03.23 |
| deB | de Bilt | Holland | 06260; 062600 | 1902.01.01.07–2008.01.03.23 |
| Jan | Jan Mayen(Nor-Navy); Jan Mayen | Norway | 01001; 010010 | 1922.01.01.02–2008.01.03.23 |
| Nor | Nordby; Esbjerg | Denmark | 25140; 060800 | 1874.01.01.08–2008.01.03.21 |

A site usually refers to the combination of the stations listed to its right, except for Pre, which is a single station site and used only to fill in the data gap of the Abe site (see Sect. 2 for details)

As detailed in the "Appendix A", each SLP data series is first screened for large random errors. As a result, a total of 45 erroneous/suspicious values were identified and excluded or corrected (see Fig. 8; Table 5).

The pressure triangles that are formed from the 11 sites used in this study are listed in Table 2 and shown in Fig. 1.

Table 2 Pressure triangles analyzed in this study

| Alexandersson's triangles | Supplement triangles | Combined or new triangles |
|---|---|---|
| Jan-Sty-Bod (JSB) | | |
| Tor-Sty-Bod (TSB) | | |
| Bod-Tor-Ber (BTB) | | |
| Abe-Tor-Ber (ATB) | Pre-Tor-Ber (PTB) | APTB = ATB + PTB |
| Ber-Abe-Ves (BAV) | Ber-Pre-Ves (BPV) | BAPV = BAV + BPV |
| Nor-Tor-Ber (NTB) | | |
| deB-Abe-Ves (DAV) | deB-Pre-Ves (DPV) | DAPV = DAV + DPV |
| Abe-Val-deB (AVD) | Pre-Val-deB (PVD) | APVD = AVD + PVD |
| Val-Tor-Abe (VTA) | Val-Tor-Pre (VTP) | VTAP = VTA + VTP |
| Val-Sty-Tor (VST) | | |
| | | Jan-Sty-Tor (JST) |
| | | Jan-Tor-Bod (JTB) |
| | | Bod-Ber-Ves (BBV) |

For each triangle, the three sites are listed in the order of site 1, 2, and 3 (see "Appendix B"). The standardized percentiles of geo-winds for each combined triangle are obtained from averaging the standardized percentiles over the related two triangles, e.g., APTB from averaging over ATB and PTB

For each triangle, the geostrophic wind speeds (referred to as geo-winds hereafter) are calculated from instantaneous SLP values for the same hour at the three sites that form the triangle (see "Appendix B" for details). The first ten triangles in Table 2 are very similar to the ten that were analyzed by Alexandersson et al. (2000) for this region (except that we use the combined triangles in the third column in place of those in the first column); our results can therefore be compared with theirs. We also added three new triangles: JST and JTB, which cover the same area as triangles JSB and TSB but enable us to distinguish between the eastern and western parts of that area, and BBV over Norway. Note that the new triangles JST and JTB are also more comparable with the other triangles in terms of spatial (zonal) scale than triangles JSB and TSB.

Since the hours of observation are often different among the three sites of a triangle, we fit natural splines to the instantaneous SLP data series at each site and then evaluate the fitted splines 3-hourly data points at hours 00, 03,…,8, 21 of each day. These calculated values at each site are used as the site's SLP series. Note that the fitted natural spline goes through each and every point of the SLP data series for each site. Thus, if there is an observed value at any of the 3-hourly data points, this value is retained in the derived 3-hourly SLP data series. The fitted spline is used to interpolate an unobserved 3-hourly value only if the observations before and after the interpolation point are separated by no more than 7 h. Also, any 24-h period with less than 2 observations was excluded from our analysis (i.e., such periods were set to missing).

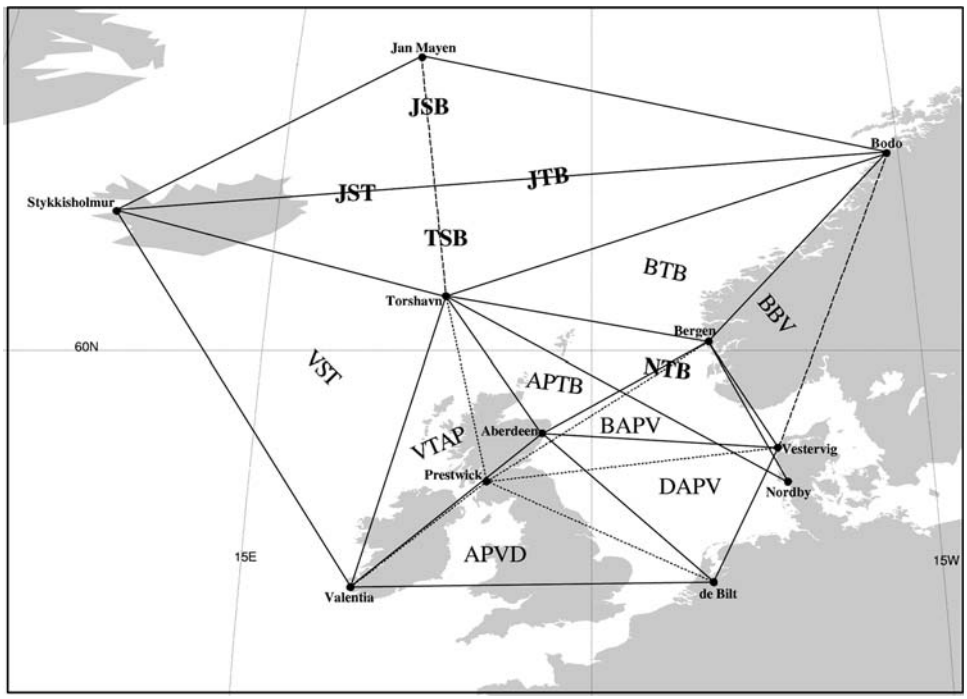


Fig. 1 The pressure triangles that are analyzed in this study. All *triangles* with a *dashed line* are new, not analyzed in Alexandersson et al. (2000). All *triangles* with a *dotted line* are supplementary triangles (see Sect. 2; Table 2)

For each triangle, geo-winds are calculated from the 3-hourly instantaneous SLP values at the three sites that form the triangle when none of the three values is missing. Historical lat/long changes over time at each site are taken into account in the calculation of 3-hourly geo-winds. When a site is represented by two stations, geo-winds are calculated for the two stations separately, obtaining a geo-wind series for each station. The pair of geo-wind series are plotted together and checked to ensure homogeneity of the combined series. The two stations often have overlapping data periods, which are very useful for the homogeneity check. As a result, we found only one inconsistency; station 060110 has data for period 1940–1943 that are inconsistent with the rest of the data for the Tor site. This inconsistent data segment was simply excluded from our analysis because station 06011 also has data for that period.

Annual and seasonal 95th and 99th geo-wind percentiles are derived from the 3-hourly geo-wind series for each triangle, for each year and season respectively. Each of these percentile series was standardized by removing the sample mean from the series and dividing the residuals by the standard deviation of the series, which makes the geo-wind percentile series for different triangles more comparable. The resulting series of standardized percentiles are then filtered using an 11-point Gaussian smoother, as in Alexandersson et al. (2000). The length of the Gaussian smoother was reduced at the end points of each series (i.e., for the first or last five points). Thus, the smoothed curve is not as good at these end points but are drawn out nevertheless. Note that for an end point at year $y$, the weights at all available data points in the range from $(y - 5)$ to $(y + 5)$ inclusive are rescaled so that they still add up to unity.

We also assess the long-term trend in each standardized geo-wind percentile series. Specifically, we use the Kendall test to estimate statistical significance of monotone trends, and the Kendall's slope estimator to obtain estimates of linear trends (Hirsch et al. 1982; Kendall 1955; Mann 1945). In the Kendall trend analysis, the effect of lag-1 autocorrelation on the estimates of trend magnitude and significance was also taken into account using the iterative procedure described in "Appendix A" of Wang and Swail (2001). The Kendall trend analysis is performed on each percentile series for each of the four seasons, separately. The results are summarized in Table 3 and discussed later in Sect. 3.

In addition, we also applied the seasonal Kendall test for data with serial dependence (referred to as the SKSD test hereafter; Hirsch and Slack 1984; Hess et al. 2001) to the consecutive seasonal series of standardized geo-wind percentiles. The null hypothesis for this test is that there is no trend in each and every season; and the alternative is that there is a monotone trend in one or more seasons. In other words, this is a test for an overall trend (i.e., considering all four seasons together).

Area averages of the standardized percentile series were also derived for the whole Northeast (NE) Atlantic region (JSB+TSB+BTB+APTB+BAPV+DAPV+NTB+APVD+VTAP+VST) and the North Sea area (APTB+BAVP+DAPV+NTB). These series of area averages are also subjected to the Gaussian smoothing and the trend analyses.

It is worth pointing out that the Gaussian smoothed curves much better represent the long-term variability and trends than do the linear trend estimates, especially in winter. The significance of the monotone trend is therefore considered of secondary importance and will not be discussed in great detail in this study. The estimated linear trend lines are shown later mainly to ease readers' visualization of the long-term variability and trends.

The 1948–1956 data gap at the Abe site affects five of the analyzed triangles, with the Abe site being near the center of the area covered by these triangles (Fig. 1). The resulting gaps in the geo-wind series in these triangles are filled as follows: First, the Pre site was used in place of the Abe site to form five supplementary triangles, which cover exactly the same area as the five affected triangles, as shown in Fig. 1. As a result, each affected triangle is paired with a supplementary triangle (see Table 2). These 3-hourly geo-wind series and corresponding standardized percentile series were also derived for each of the supplementary triangles. The pairs of standardized percentile series that correspond to the affected triangles and their supplementary triangles are then averaged to form new percentile series to represent the storminess conditions over the areas covered by the related pairs of triangles combined. Such an area is referred to as a combined triangle. For example, ATB is an affected triangle and PTB is the corresponding supplementary triangle; the area covered by triangles ATB and PTB combined is referred to as the combined triangle APTB (Table 2). For each year/season, the standardized 95th (or 99th) percentiles for triangles ATB and PTB are averaged to form a new 95th (or 99th) percentile to represent the storminess condition in that year/season over the combined triangle APTB. The resulting geo-wind percentile series represents historical storminess conditions over the combined triangle APTB. Note that this series has the same values as the corresponding series for triangle PTB for the period 1948–1956 (a data gap in the series for triangle ATB).

The homogeneity of the geo-wind series was analyzed using the new climate homogenization techniques PMFred and PMTred of Wang (2008a). The PMFred algorithm is for detecting mean shifts without trend change in time series of a constant linear trend and thus can be used without a reference series; while the PMTred algorithm is

Table 3 Linear trend estimates $\hat{\beta}$ obtained from the Kendall's slope estimator and the corresponding $Z$ statistics for each standardized seasonal 95th/99th percentiles of geo-winds over the indicated areas

| Region | 99th percentiles | | 95th percentiles | | 99th percentiles | | 95th percentiles | |
|---|---|---|---|---|---|---|---|---|
| | Trend | $Z$ | Trend | $Z$ | Trend | $Z$ | Trend | $Z$ |
| | DJF | | | | MAM | | | |
| JSB | 0.00311 | 0.70 | −0.00120 | −0.28 | *0.01067* | 1.84 | 0.01470 | 3.04 |
| TSB | *−0.00581* | −1.89 | *−0.00492* | −1.46 | −0.00189 | −0.75 | −0.00404 | −1.25 |
| JTB | 0.00426 | 0.82 | 0.00413 | 0.84 | 0.01094 | 2.08 | *0.01088* | 1.88 |
| JST | −0.00515 | −1.26 | −0.00512 | −1.20 | *0.01008* | 1.76 | 0.00609 | 1.19 |
| VST | −0.00325 | −1.10 | −0.00610 | −2.11 | 0.00066 | 0.23 | 0.00183 | 0.60 |
| VTAP | 0.00071 | 0.19 | −0.00222 | −0.51 | −0.00282 | −0.98 | −0.00033 | −0.11 |
| APVD | −0.00214 | −0.51 | 0.00002 | 0.01 | −0.00060 | −0.14 | −0.00229 | −0.59 |
| DAPV | 0.00052 | 0.16 | −0.00313 | −0.82 | −0.00146 | −0.36 | −0.00003 | −0.02 |
| BAPV | −0.00131 | −0.48 | −0.00160 | −0.73 | −0.00305 | −1.17 | −0.00544 | −2.20 |
| APTB | 0.00137 | 0.60 | −0.00165 | −0.72 | −0.00004 | −0.03 | 0.00055 | 0.25 |
| NTB | 0.00289 | 1.09 | −0.00017 | −0.08 | 0.00028 | 0.10 | 0.00040 | 0.13 |
| BTB | −0.00340 | −1.01 | −0.00291 | −0.86 | *0.00520* | 1.39 | 0.00206 | 0.77 |
| BBV | −0.00295 | −0.84 | −0.00312 | −0.79 | −0.00183 | −0.55 | *−0.00474* | −1.35 |
| NE Atlantic | −0.00032 | −0.26 | −0.00250 | −1.34 | −0.00142 | −0.78 | −0.00149 | −0.79 |
| North Sea | 0.00126 | 0.59 | −0.00158 | −0.82 | −0.00207 | −0.85 | −0.00163 | −0.80 |
| | JJA | | | | SON | | | |
| JSB | 0.00103 | 0.23 | −0.00358 | −0.81 | 0.00053 | 0.13 | 0.00427 | 0.91 |
| TSB | −0.00044 | −0.20 | −0.00105 | −0.33 | 0.00359 | 1.16 | 0.00146 | 0.46 |
| JTB | −0.00350 | −0.75 | −0.00256 | −0.55 | 0.00290 | 0.66 | −0.00060 | −0.09 |
| JST | −0.00252 | −0.68 | −0.00316 | −0.75 | 0.00234 | 0.57 | −0.00164 | −0.39 |
| VST | 0.00107 | 0.50 | −0.00224 | −0.80 | 0.00313 | 1.23 | 0.00038 | 0.10 |
| VTAP | −0.00174 | −0.59 | 0.00039 | 0.13 | 0.00002 | 0.01 | −0.00025 | −0.08 |
| APVD | *−0.00523* | −1.66 | −0.00852 | −2.52 | −0.00339 | −0.90 | 0.00212 | 0.62 |
| DAPV | *−0.00539* | −1.62 | −0.01008 | −3.03 | −0.00178 | −0.50 | −0.00126 | −0.37 |
| BAPV | −0.00727 | −3.06 | −0.00855 | −3.36 | *−0.00279* | −1.54 | −0.00274 | −1.34 |
| APTB | −0.00336 | −1.26 | −0.00194 | −0.74 | −0.00203 | −1.25 | −0.00083 | −0.51 |
| NTB | −0.00398 | −1.27 | −0.00257 | −0.89 | 0.00095 | 0.43 | −0.00032 | −0.14 |
| BTB | −0.00197 | −0.54 | −0.00140 | −0.38 | 0.00356 | 0.95 | 0.00274 | 0.72 |
| BBV | *−0.00555* | −1.75 | *−0.00479* | −1.62 | 0.00002 | 0.01 | 0.00113 | 0.39 |
| NE Atlantic | −0.00375 | −2.13 | −0.00406 | −2.51 | −0.00129 | −1.01 | −0.00136 | −0.93 |
| North Sea | −0.00459 | −2.01 | −0.00534 | −2.62 | −0.00170 | −1.13 | −0.00152 | −0.80 |

Trends of $p$ values $\geq$ 0.95 and 0.80 are shown in bold and italic, respectively. The corresponding $Z$ critical values are $Z_{1-\frac{0.05}{2}} = 1.96$ and $Z_{1-\frac{0.20}{2}} = 1.28$, respectively (two-sided test)

for detecting mean shifts in time series of zero trend and thus often needs to be used with a good homogeneous reference series (Wang 2008a). Both algorithms were used in this study. In order to find a homogeneous series for use as a reference series, we first applied the PMFred algorithm (Wang 2008a, b; Wang and Feng 2007) to the consecutive monthly mean geo-wind series for each of the 13 triangles listed in Table 2. As a result, the JSB, JST, and VST series are found to be homogeneous at the 5% significance level (i.e., $\alpha = 0.05$), among which the VST series is the longest series and thus chosen as the reference series. The PMTred algorithm (Wang 2008a; Wang and Feng 2007) was then applied to each of the other 12 series, using the VST series as reference series. The results indicate that most of the series are homogeneous, with the exception of two significant changepoints in the DAPV and VTAP series, which could be associated with the period of missing data (1948–1956) at the Abe site (the data gap was filled in using the Pre site data). Thus, we adjusted these series for two changepoints, at the very end of 1947 and 1956, respectively, with the adjustments being estimated from the base-minus-reference series (the base

series is the series being adjusted/tested). Since discontinuities in the Abe/Pre combined series could affect all five triangles that involve this series (i.e., VTAP, APVD, DAPV, BAPV, and APTB), we performed the adjustments for each of these five geo-wind series, although the adjustments are small for all but the DAVP series. After these adjustments, all the geo-wind series are judged to be homogeneous. These adjustments were done prior to calculation of geo-wind percentiles, Gaussian filtering and trend analyses.

## 3 Long-term trends and variability of storminess

First of all, as shown in Fig. 2, our area averaged standardized annual 99th and 95th geo-wind percentile series are very similar to those shown in Fig. 2 of Alexandersson et al. (2000), although our data sources and preparation procedures are slightly different from theirs (in particular, we interpolate the pressure data series to form 3-hourly series, and we use five combined triangles in place of the five triangles that involve the Abe site, see Table 2). In terms of these annual geo-wind percentiles, the recent storminess maximum (in the early 1990s) is indeed at about the same level as the maximum in the early 1880s or around 1905, and the lowest level of storminess in the period of record is seen in the mid-1960s, as reported in Alexandersson et al. (1998, 2000), WASA (1998), and Matulla et al. (2008). Decadal or longer time scale variability in storminess is very profound in this region. The latest upward phase of storminess starts around 2005. In terms of monotone trends, the Kendall test identifies a downward trend of at least 5% signifiance in both the 99th and 95th percentile series (see Fig. 2, caption).

However, as shown in Fig. 3 and Table 3, there are large seasonal and regional differences in trends and variability. A common characteristic is that large amounts of decadal or longer time scale variability are evident in all seasons throughout the region. In winter (DJF), storminess appears to have strengthened in the North Sea area while it has declined in the western area and over the Norwegian Sea (Fig. 3a). The northern triangles JST and JTB also show trends of opposite sign in winter: an upward trend in the eastern area and a downward trend in the western area (Fig. 3a), revealing a zonal gradient in trends in this region. This gradient is not evident when analyzing triangles JSB and TSB as in Alexandersson et al. (2000). The latter pair of triangles, which span a much larger zonal distance than all other triangles analyzed, have trends of opposite sign in all seasons but autumn (Table 3), showing a meridional trend gradient in this region (increases over JSB and decreases over TSB). The new triangles JST and JTB, which sample the zonal trend gradient, are more comparable with all of the other triangles in terms of zonal scale than triangles JSB and TSB, and thus are preferred in this study. In summer (JJA), storminess conditions appear to have declined in most parts of the NE Atlantic region (Fig. 3b). In the transition seasons, the storminess trend is characterized by increases in the northern part of the region and slight decreases over the North Sea area (Figs. 3c, d). The

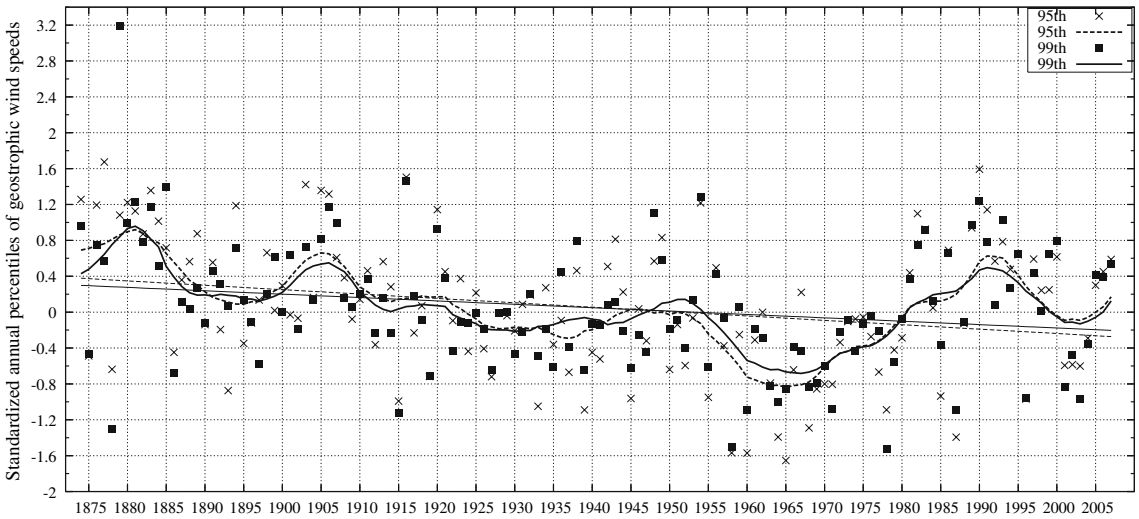


Fig. 2 NE Atlantic region area averages of standardized annual 99th and 95th percentiles of 3-hourly geostrophic wind speeds, and the corresponding Gaussian low-pass filtered curves and linear trends. The Kendall's slope estimates for the 99th and 95th percentile series are $\hat{\beta}_{99th} = -0.00377 (Z = 2.25 > Z_{1-\frac{0.05}{2}})$ and $\hat{\beta}_{95th} = -0.00489 (Z = 2.13 > Z_{1-\frac{0.05}{2}})$, respectively

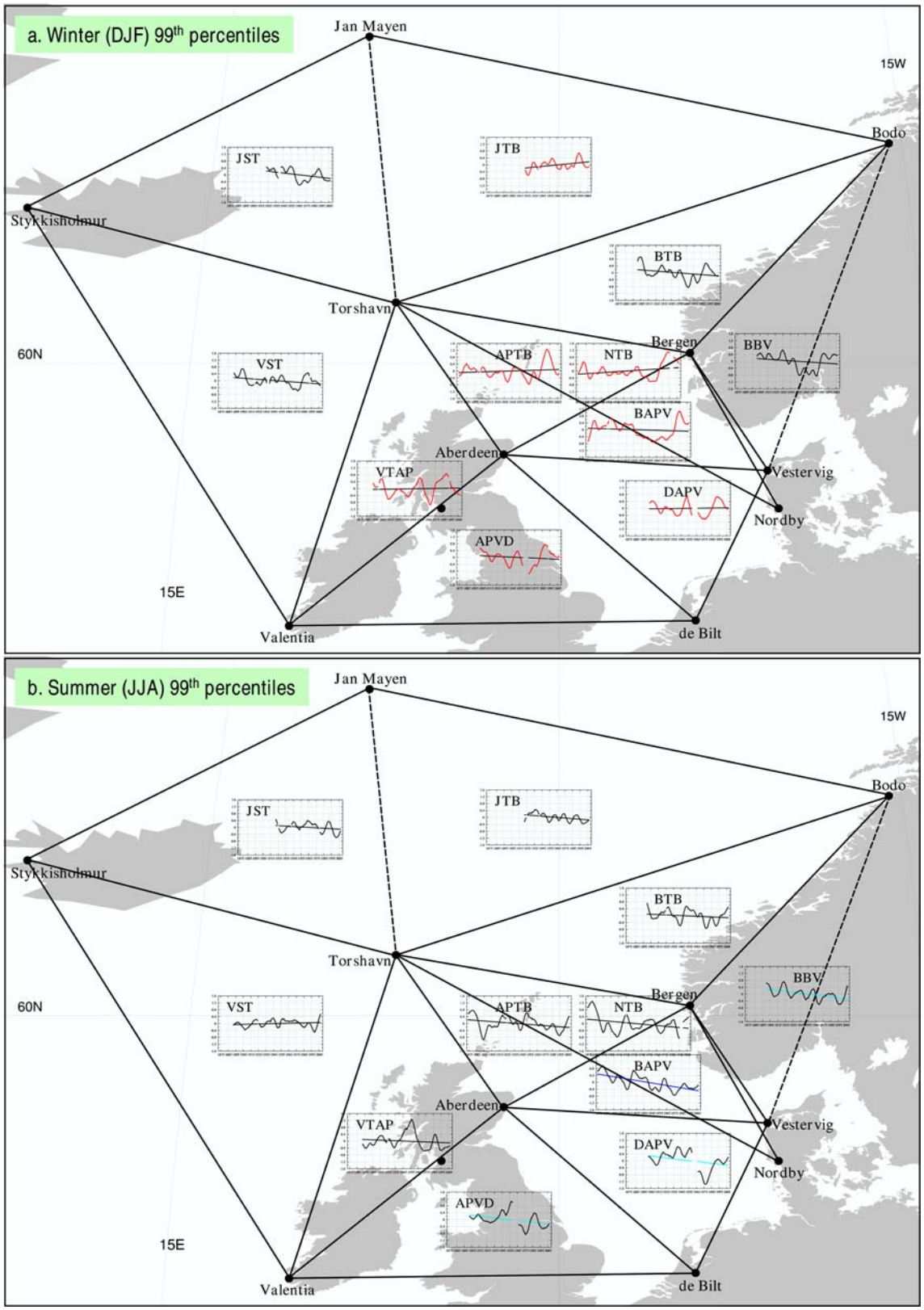


Fig. 3 The Gaussian low-pass filtered curves and the estimated linear trends of the indicated seasonal 99th percentiles of geo-winds for the 11 pressure triangles. *Red* and *magenta* (*blue* and *cyan*) trend lines indicate upward (downward) trends of $p$ values $\geq 0.95$ and 0.80, respectively. The curves with an unprecedented maximum in the early 1990s are also shown in *red*

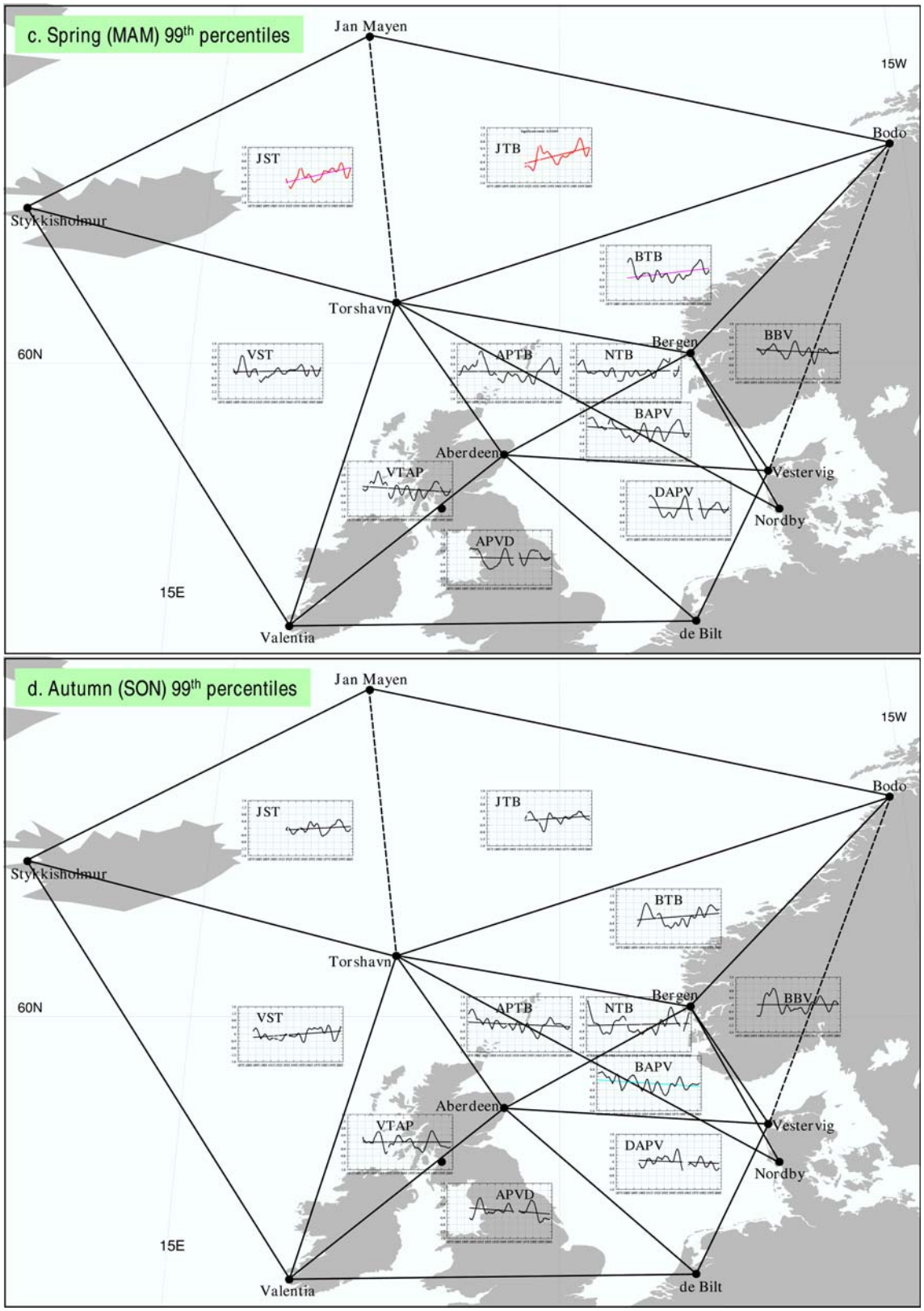


Fig. 3 continued

increases in the north are of some statistical significance in spring (Fig. 3c; Table 3).

The North Sea area triangles (APTB, BAPV, DAPV, and NTB) share similar long-term variability in winter (Fig. 3a), and also in summer (Fig. 3b). Thus, we also calculated area averages of the standardized seasonal percentiles over the four triangles. As shown in Fig. 4, at the decadal or longer-time scales, winter storminess conditions often fluctuate out of phase with summer storminess conditions (e.g., early 1960s and early 1990s). In particular, the most recent storminess maximum (in the early 1990s) is seen only in winter and spring (Figs. 3a, c, 4a), while the earliest maximum (around 1880s) is not seen in winter but is most evident in summer (Figs. 3, 4). Looking at the annual percentiles alone (as in Fig. 2; Alexandersson et al. 2000), one would conclude that the latest storminess maximum is at about the same level as the earliest storminess maximum, without realizing that this is comparing the highest winter storminess level with the highest summer storminess level in the period of record, while winter and summer storminess conditions have undergone very different long-term variability and trends. Note that the earliest maximum of summer storminess is seen only in the North Sea area; other areas have no data for this early period (before 1892; see Fig. 3). This is another reason for us to look at the North Sea area separately.

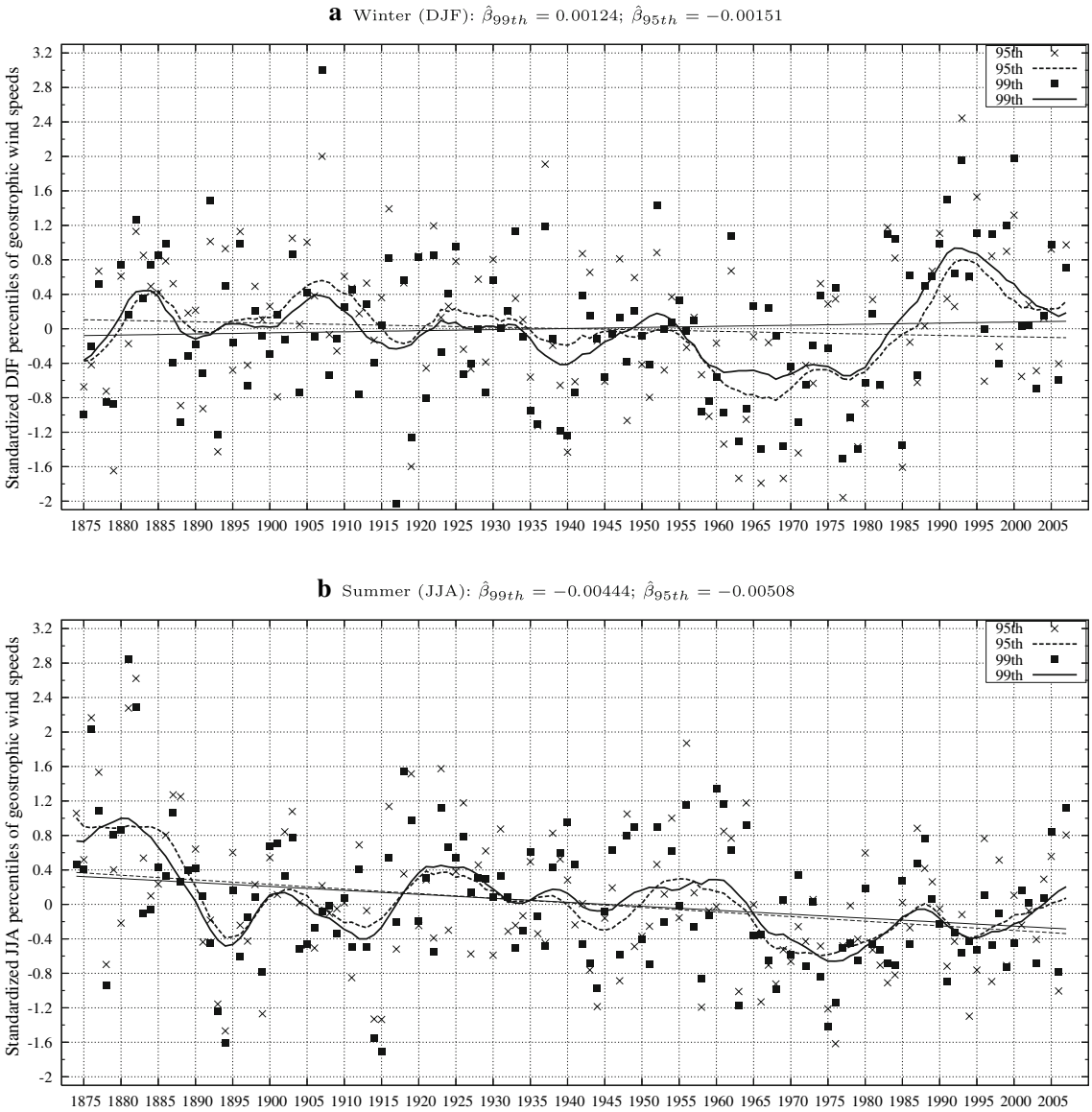


Fig. 4 The same as in Fig. 2 but for area averages of the standardized seasonal 99th and 95th percentiles of geo-winds in the North Sea area (APTB+BAPV+DAPV+NTB)

In terms of monotone trends, at the 5% significance level, the SKSD tests on the North Sea area averaged consecutive seasonal percentile series suggest that there is a significant monotone trend in one or more of the four seasons in both the 99th and 95th percentiles ($Z = -2.35$, $Z = -3.06$). Further, the Kendall tests (two-sided) on the series for individual seasons separately identify a significant downward trend in the summer 99th and 95th percentile series, but no significant monotone trends in the other seasons (see the North Sea rows in Table 3). Note that the estimated linear trend is positive for the winter 99th percentile series, but negative for all the other North Sea series (Table 3). In particular, as shown in Fig. 4a, winter storminess in the North Sea area shows an unprecedented high level in the early 1990s, and its most recent low level (around 2005) did not go below the long-term mean level. For the winter 99th percentiles, the Gaussian smoothed curve fluctuates between −0.6 and 0.4 before 1986, but between 0.2 and 0.9 in the las two decades. Also, the individual geo-wind percentiles did not fall below −0.8 standard deviation during the last two decades (Fig. 4a). In all seasons but winter, storminess in the North Sea area appears to have a downward trend, which is most notable in summer (Figs. 3b–d, 4b; also Table 3).

In the British Isles area, the early 1990s maximum in winter storminess is also slightly higher than the maximum around 1905 (see APVD and VTAP in Fig. 3a). For the period 1957–2003, the winter storminess conditions as inferred from the extreme geo-winds (Fig. 3a) are consistent with the seasonal counts of severe storms in the United Kingdom (Alexander and Tett 2005), showing a calm period from the late 1950s to around 1980 and a recent maximum around 1990. The largest multi-decadal variations in storminess in this area are seen in summer, ranging from the record high level around 1956 to the lowest level in the mid-1970s (Fig. 3a). This multi-decadal variability is not seen in the other seasons in this area, nor in the other parts of the NE Atlantic region.

In terms of the averages over the whole NE Atlantic region, seasonal differences are less apparent in general, except that the storminess maximum at the end of the 19th century is still most evident in summer, and that the latest maximum in the early 1990s is most profound in winter but not seen in summer and fall (not shown).

Further, it is important to point out that these geo-winds well approximate real surface winds. In comparison with the corresponding geo-wind percentile series, Fig. 5 shows the NE Atlantic area averaged standardized seasonal 99th percentiles of surface wind speeds (WsP99) taken from the ERA40 reanalysis (Uppala et al. 2005), with the area average being taken over 10 gridpoints, each of which is near one of the 10 sites used to calculate the geo-winds. Clearly, the surface wind speeds as represented in the ERA40 reanalysis correspond very well to the geo-wind speeds derived from surface pressure observations at the 10 sites in this region, especially in terms of the low-frequency variability of wind speeds.

## 4 Storminess conditions and the NAO

Several studies have reported significant relationships between the North Atlantic Oscillation (NAO) and storminess conditions in the North Atlantic domain (e.g., Wang et al. 2006b; Jung et al. 2003; Ulbrich and Christoph 1999). The NAO-storminess relationship is also explored in this section.

We use the NAO index that is based on the difference of normalized SLP between Ponta Delgada, Azores and Stykkisholmur/Reykjavik, Iceland (Hurrell and van Loon 1997; Hurrell 1995). We downloaded the monthly NAO index series for the period from January 1865 to March 2003 from http://www.cgd.ucar.edu/cas/jhurrell/indices.data.htm. Since the Ponta Delgada/Observatory station (ID: 08513) ceased to report surface pressure observations in September 2004, we use SLP data from a nearby station, Ponta Delgada/Norde (ID: 08512), to update Hurrell's NAO index series to April 2008, using the means and standard deviations kindly provided by James W. Hurrell (NCAR, USA). The updated monthly NAO index series was found to be homogeneous by the PMFred test (Wang 2008a); the use of data from a nearby station does not introduce any discontinuity in the series. Inter-comparison of the pair of NAO index series that are calculated from the two Ponta Delgada stations over their common period of data, 1973–2003, reveals only trivial random differences. The seasonal mean NAO index series are derived from the monthly series for each of the four seasons, separately. Correlations for the period 1875–2007 between seasonal NAO indices and the area averaged standardized seasonal percentiles of geo-winds over the NE Atlantic region and the North Sea area are calculated and reported in Table 4 (sample size $N = 131$ for winter and $N = 132$ for the other seasons).

As shown in Table 4, storminess conditions in the NE Atlantic region are highly significantly correlated with the simultaneous NAO index in winter ($p = 1 - \alpha > 0.9999$), and also in spring ($p > 0.9990$). The higher the NAO index, the rougher the NE Atlantic storminess conditions in winter and spring (Table 4). As shown in Fig. 6, there is a closer winter NAO-storminess relationship in the second half of the period than in the first half; they were slightly out of phase during the first two decades but particularly consistent with each other during the last two decades. In summer, the correlations are much lower, especially for the North Sea area; but they are still of moderately high

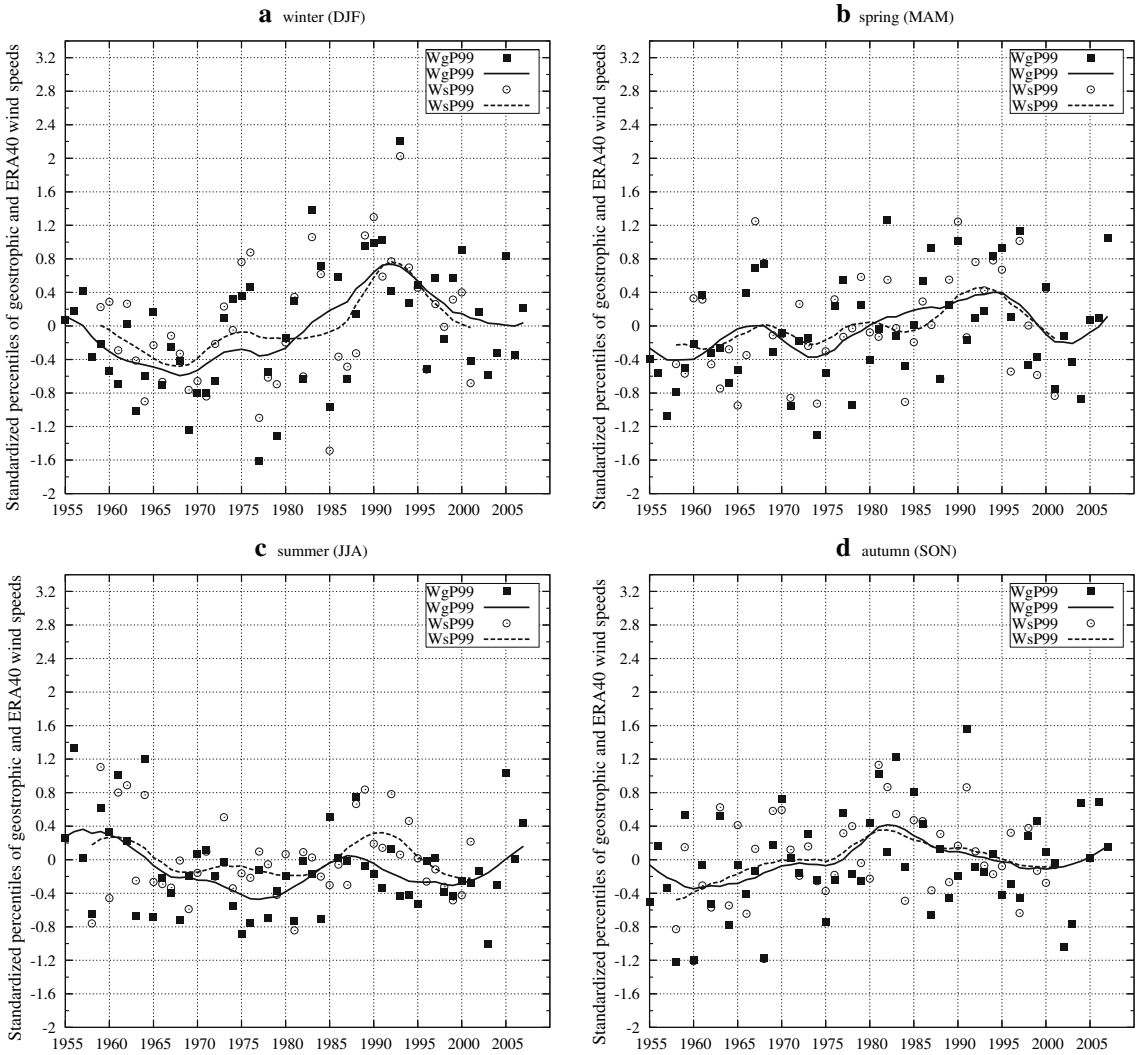


Fig. 5 NE Atlantic region area averages of standardized seasonal 99th percentiles of geo-wind speeds (WgP99) and surface wind speeds (WsP99; taken from ERA40), and the corresponding Gaussian low-pass filtered curves

Table 4 Correlations between seasonal NAO indices and the area averaged standardized seasonal percentiles of geo-winds over the NE Atlantic region and the North Sea area, for the period from 1875 to 2007

| | | DJF | MAM | JJA | SON |
|---|---|---|---|---|---|
| NE Atlantic | 99th | 0.570 | 0.302 | 0.213 | 0.070 |
| | 95th | 0.667 | 0.406 | 0.248 | 0.118 |
| North Sea | 99th | 0.547 | 0.283 | 0.168 | 0.079 |
| | 95th | 0.636 | 0.358 | 0.123 | 0.084 |

Correlations of at least 5% significance are shown in bold (the 95 and 99.99% critical values of correlation are 0.143 and 0.317, respectively)

statistical significance in terms of the whole NE Atlantic region ($p = 0.995$–$0.999$; see Table 4). In autumn, however, there is no significant relationship between the NAO and storminess conditions in the NE Atlantic region, although the correlations are still positive (Table 4, last column).

## 5 Concluding remarks

We have updated the studies by Alexandersson et al. (1998, 2000), extending the analysis period up to January 2008, and have explored the seasonal and regional differences of storminess conditions in the NE Atlantic region in detail. The results of our analysis show that storminess conditions in this region have undergone profound decadal or longer time scale fluctuations, with considerable seasonal and regional differences. The most notable differences are seen between winter and summer, and between the North Sea area and other parts of the region. In

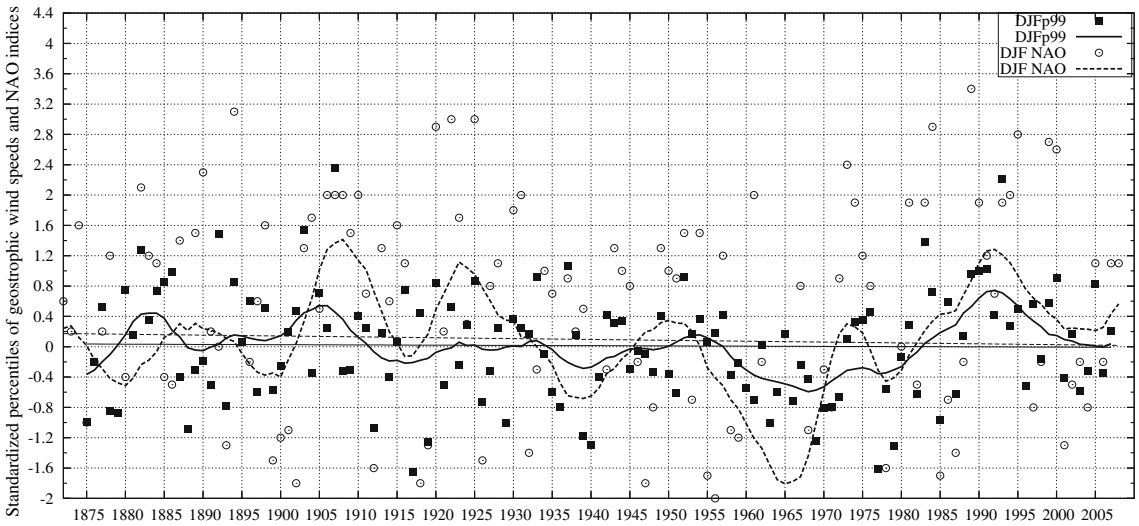


Fig. 6 The same as in Fig. 2 but for the area averages of the standardized winter 99th percentiles of geo-winds over the NE Atlantic region, in comparison with the seasonal mean NAO index series (Hurrell 1995) and its 11-point Gaussian smoothed curve and Kendall's slope estimate

particular, winter storminess shows an unprecedented maximum in the early 1990s in the North Sea area and a steady upward trend over the northeastern triangle JTB, while it appears to have declined in the western area (triangles JST and VST), showing a maximum in the Norwegian area in the early 1990s that is at about the same level as the maximum around 1905. In summer, storminess appears to have declined in most parts of the NE Atlantic region, except that the southwestern triangles (VST and VTAP) show no notable trends. In the transition seasons, the storminess trend is characterized by increases in the northern part of the region and decreases in the southeastern part, with increases in the north being more noticeable in spring.

The question of whether there is an anthropogenic contribution to changes described in the previous paragraph remains open. In a recent detection study that compares observationally based estimates of changes in atmospheric storminess (as inferred from geo-wind energy) and ocean wave heights with estimates derived from multi-model simulations of climate change driven with historical external forcing from both anthropogenic and natural sources, Wang et al. (2008) have shown that the atmospheric storminess and ocean wave heights have increased in boreal winter over the past half century in the northeast North Atlantic (and have decreased in more southerly northern latitudes), and that these trend patterns contain a detectable response to anthropogenic and natural forcing combined. In the same study, they also found that the effect of external influence is strongest in the winter hemisphere, that is, in the northern hemisphere in January-February-March and in the southern hemisphere in July–August–September. These results are consistent with the results shown in this study, though the effect of

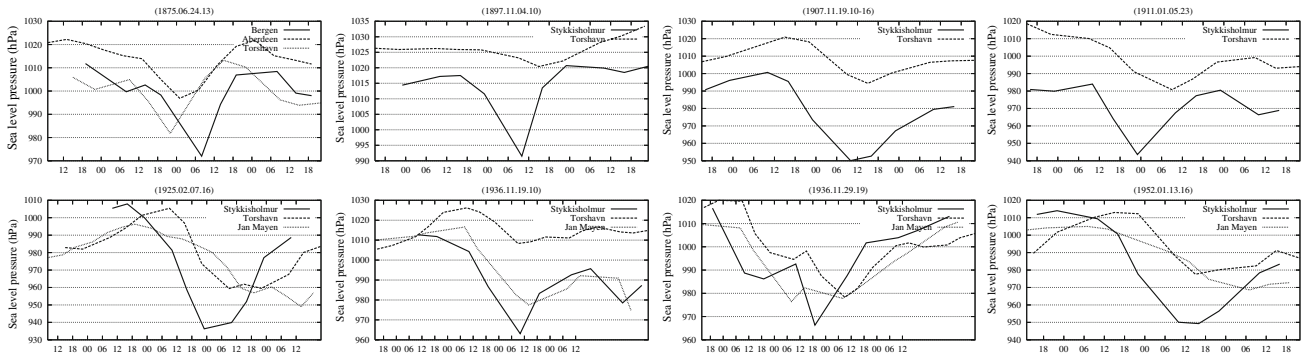


Fig. 7 Segments of suspicious SLP values (i.e., the lowest values in the *solid curves*), in comparison with the corresponding segments from two/one nearest stations if available. The *x*-axis is the hour of observation. These suspicious values are most likely true extremes and hence kept unchanged

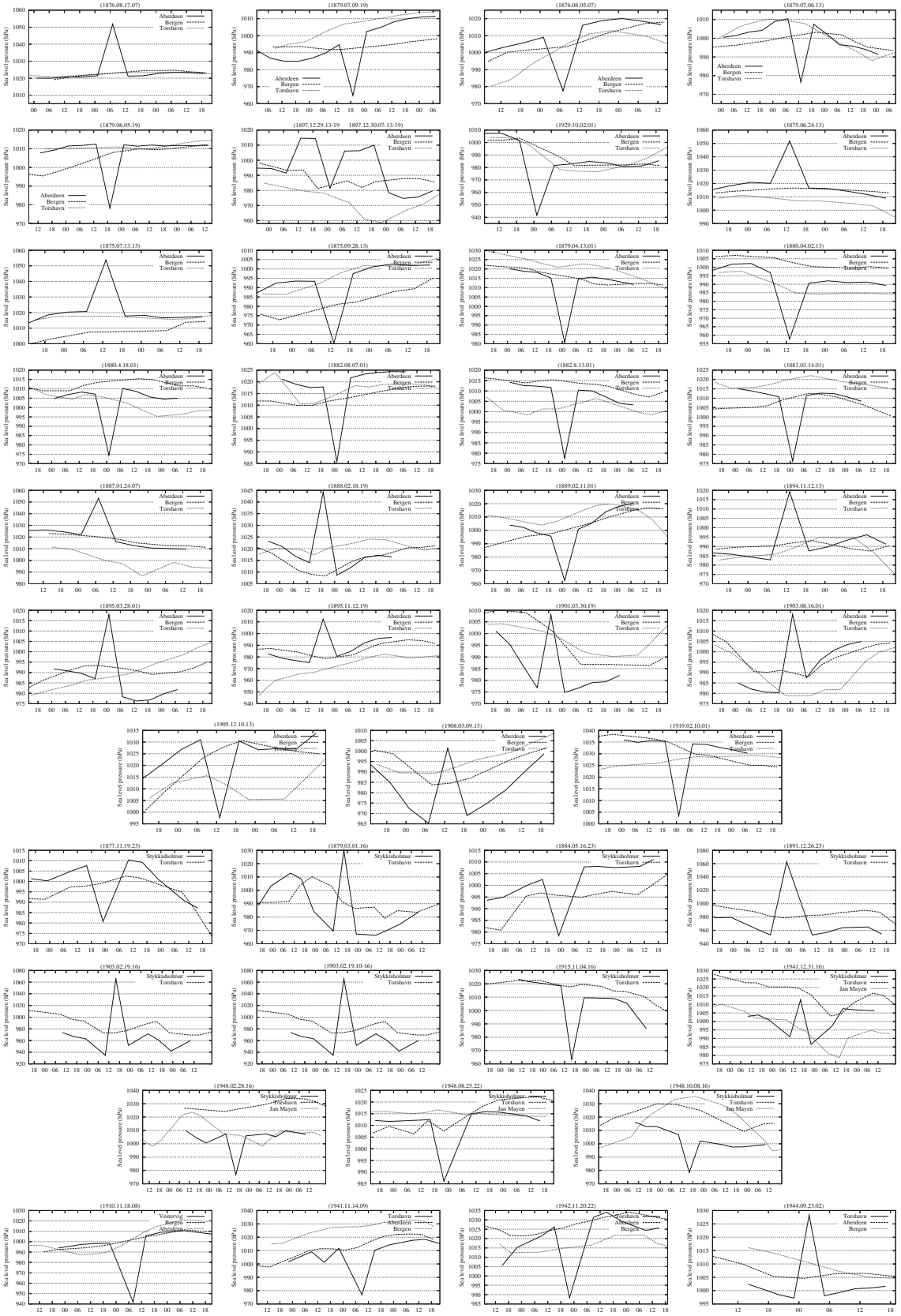


Fig. 8 The same as in Fig. 7 but these suspicious SLP values (i.e., the outliers in the *solid curves*) are most likely erroneous and hence are set to missing or corrected when possible (see Table 5)

Table 5 Erroneous/suspicious SLP values that were either corrected or set to missing

| Station ID | Date | SLP (hPa) | Treatment | Station ID | Date | SLP (hPa) | Treatment |
|---|---|---|---|---|---|---|---|
| 03091 | 1875.06.24.13 | 1051.8 | Set to missing | 03091 | 1897.12.30.19 | 1010.0 | Set to missing |
| 03091 | 1875.07.13.13 | 1053.7 | Set to missing | 03091 | 1901.03.30.19 | 1008.1 | Set to missing |
| 03091 | 1875.09.28.13 | 960.3 | Set to missing | 03091 | 1903.08.16.01 | 1018.0 | Set to missing |
| 03091 | 1876.08.05.07 | 977.5 | Set to missing | 03091 | 1905.12.10.13 | 997.7 | Set to missing |
| 03091 | 1876.08.17.07 | 1051.8 | Set to missing | 03091 | 1908.03.09.13 | 1001.4 | Set to missing |
| 03091 | 1879.04.13.01 | 980.8 | Set to missing | 03091 | 1919.02.10.01 | 1003.4 | Set to missing |
| 03091 | 1879.06.05.19 | 978.2 | Set to missing | 03091 | 1929.10.02.01 | 941.7 | 991.7 |
| 03091 | 1879.07.06.13 | 976.5 | Set to missing | | | | |
| 03091 | 1879.07.09.19 | 964.8 | 994.8 | 21100 | 1910.11.18.08 | 941.7 | Set to missing |
| 03091 | 1880.04.02.13 | 957.8 | Set to missing | | | | |
| 03091 | 1880.04.18.01 | 974.5 | Set to missing | 06011 | 1941.11.14.09 | 976.8 | Set to missing |
| 03091 | 1882.08.07.01 | 985.9 | Set to missing | 06011 | 1942.11.20.22 | 988.4 | Set to missing |
| 03091 | 1882.08.13.01 | 977.6 | Set to missing | 06011 | 1944.09.23.02 | 1028.3 | Set to missing |
| 03091 | 1883.03.14.01 | 976.4 | Set to missing | | | | |
| 03091 | 1887.01.24.07 | 1053.2 | Set to missing | 04013 | 1877.11.19.23 | 980.7 | Set to missing |
| 03091 | 1888.02.18.19 | 1044.2 | Set to missing | 04013 | 1879.03.01.16 | 1029.9 | Set to missing |
| 03091 | 1889.02.11.01 | 962.5 | Set to missing | 04013 | 1884.05.16.23 | 978.4 | Set to missing |
| 03091 | 1894.11.12.13 | 1019.2 | Set to missing | 04013 | 1891.12.26.23 | 1062.7 | Set to missing |
| 03091 | 1895.03.28.01 | 1017.9 | Set to missing | 04013 | 1903.02.19.16 | 1065.5 | Set to missing |
| 03091 | 1895.11.12.19 | 1012.4 | Set to missing | 04013 | 1915.11.04.16 | 963.5 | Set to missing |
| 03091 | 1897.12.29.13 | 1014.6 | Set to missing | 04013 | 1941.12.31.16 | 1012.7 | Set to missing |
| 03091 | 1897.12.29.19 | 1014.4 | Set to missing | 04013 | 1948.02.28.16 | 976.9 | Set to missing |
| 03091 | 1897.12.30.07 | 1006.1 | Set to missing | 04013 | 1948.08.25.22 | 986.1 | Set to missing |
| 03091 | 1897.12.30.19 | 1010.0 | Set to missing | 04013 | 1948.10.08.16 | 978.5 | Set to missing |

anthropogenic forcing was not separated from that of natural forcing in the detection study. In the mean time, several recent studies have shown evidence of an increase in intense cyclone activity (mostly in winter) in the NE Atlantic region under anthropogenic climate change. For example, Bengtsson et al. (2006) and Pinto et al. (2007) reported enhanced cyclone intensities near the British Isles. Leckebusch and Ulbrich (2004) and Leckebusch et al. (2006) detected a regional increase of extreme cyclones in the NE Atlantic region in both the Hadley Centre and the ECHAM GCMs. Ulbrich et al. (2008a) analyze the storm tracks in an ensemble of 23 runs out of 16 different coupled GCMs and confirm a greenhouse gas induced increase of cyclone activity over this region. Under anthropogenic climate change conditions, the number of intense cyclones in the NE Atlantic region (especially the British Isles) increases in most climate models (Ulbrich et al. 2008b). Comparison of the climate model simulations for the twentieth century with the station SLP based results presented in this study is on-going and will be reported in a separate study.

In winter and spring, the NE Atlantic storminess conditions are found to be highly significantly correlated with the simultaneous NAO index; the higher the NAO index, the rougher the storminess conditions. In summer, the positive NAO-storminess relationship is still statistically significant ($p = 1 - \alpha = 0.995$–$0.999$), though less strongly in winter and spring. However, there is no significant correlation between the NAO and autumn storminess conditions in the NE Atlantic region.

We have noticed that the configuration of the triangles is important, because depending upon configuration spatial gradients in trends might not be detected, while too large triangles tend to mask differences among different parts of the triangle area. It is important to configure the triangles in such a way that they are of similar spatial scale (to the extent allowed by data availability). For example, triangles JSB and TSB, which span the largest zonal distance of the entire region analyzed, mask the zonal trend gradient that was diagnosed by analyzing triangle JST and JTB (Sect. 3). Also, our interpolation of the SLP data to form 3-hourly series considerably increases the number of simultaneous SLP values for the triplet of sites in a triangle for the early period, and thus makes the sampling rate of 3-hourly geowinds more homogeneous over the period of record, resulting in more accurate representation and diagnosis of

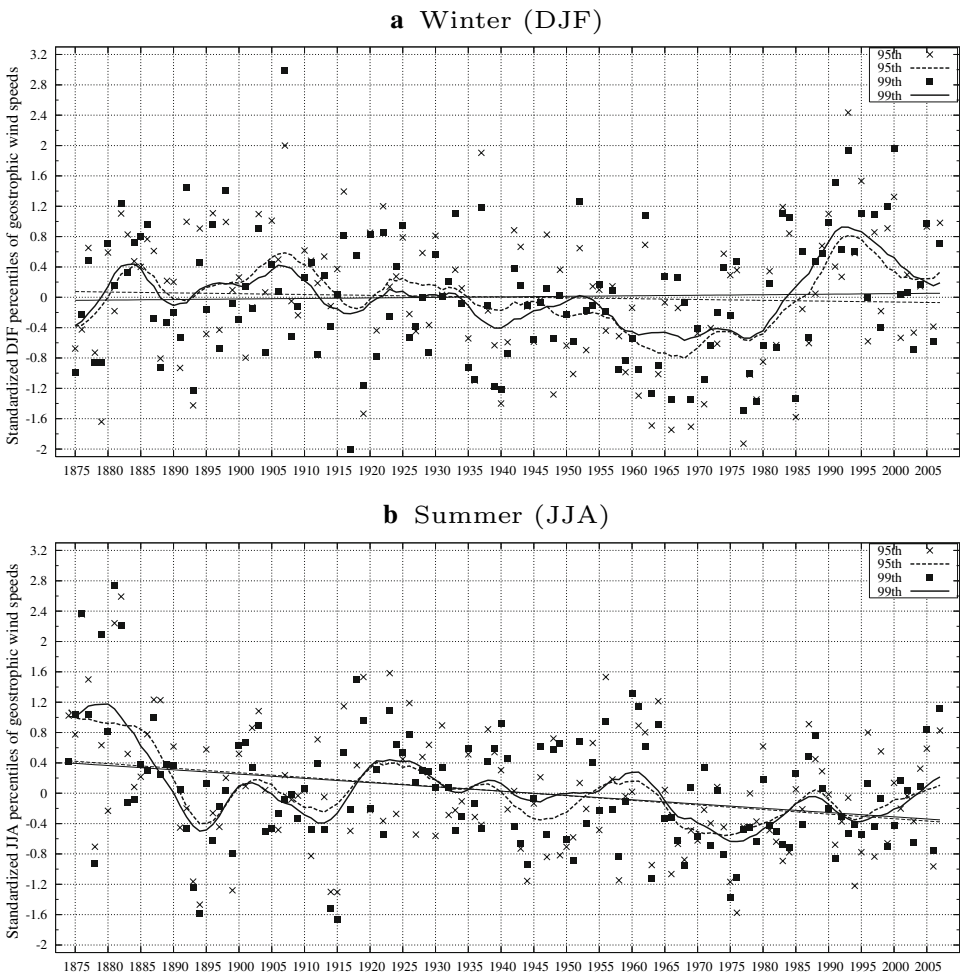


Fig. 9 The same as in Fig. 4 but these are derived from the original SLP data, leaving the suspicious/erroneous SLP values (listed in Table 5) in the series unchanged

storminess conditions, especially in terms of long-term variability and trends.

Acknowledgments The authors are very grateful to Dr. Gil Compo and other members of GCOS/WCRP AOPC/OOPC (Atmosphere/Ocean Observation Panel for Climate) Working Group on Surface Pressure for providing us with the Integrated Surface Pressure Databank, which includes all the pressure data we analyzed in this study. The authors wish to thank Mr. Tommy Jang and Ms. Hui Wan for their help in downloading and extracting the data from the database. The authors also wish to acknowledge Mr. Torben Schmith of Danish Meteorological Institute for providing Val R. Swail his FORTRAN codes for calculating geostrophic wind speeds from pressure triangles, which we have modified slightly and used in this study. The authors also wish to thank Drs. Xuebin Zhang and Seung-Ki Min for their useful internal review of an earlier version of this manuscript, and the two anonymous reviewers for their helpful review comments.

## Appendix A: Erroneous/suspicious SLP values

For any sea level pressure (SLP) series $\{P_i\}$ $(i = 1,2,\ldots,N)$, if $|P_{i-1}-P_i| > 20$ hPa and $|P_{i+1}-P_i| > 20$ hPa, the $i$th observation $P_i$ is considered a suspicious value. The 20 hPa threshold was selected considering the typical intervals between two consecutive observations in the early period (typically 8 h on average, i.e., three observations per day) and the limits for pressure tendency check used by Environment Canada [including 14.9 hPa (5 h)$^{-1}$ and 16.9 hPa (6 h)$^{-1}$; Environment Canada 2004]. The segment of observations, $\{P_i-5,P_i-4,\ldots,P_i,\ldots,P_i+4,P_i+5\}$, is checked against the corresponding segment of observations at the available nearest stations (e.g., Aberdeen is checked against Bergen and Torshavn), to determine whether the suspicious value is erroneous or not. Indeed, some of these suspects turn out to be true SLP values (e.g., those shown in Fig. 7) and are thus kept unchanged, while others are apparently erroneous. As a result, a total of 45 erroneous/suspicious values were identified; all of which are shown in Fig. 8, in comparison with the corresponding observations available at two nearest stations (only one station available in some cases). As detailed in Table 5, these values are either set to missing or corrected when possible. Most of these suspicious values are seen in the early period of the record (mostly in the late 19th century).

Note that the exclusion/correction of the suspicious SLP values listed in Table 5 makes a few outliers disappear, for example, the few outliers that show very high summer storminess around 1880s in Fig. 9b are not seen in Fig. 4b. However, the general characteristics of the decadal or longer time scale storminess variability are not significantly affected by the exclusion/correction (also see Figs. 4b, 9b). This is not surprising because the exclusion/correction of random errors are not expected to bias the results systematically.

## Appendix B: Calculation of geostrophic wind speeds

For each pressure triangle, the geostrophic wind speeds (also referred to as geo-winds) are calculated from instantaneous SLP values for the same hour at the three sites that form the triangle (say site 1, 2, and 3). Let $P_1$, $P_2$, and $P_3$ denote the three instantaneous SLP values of the same hour at the three sites (site 1, 2, and 3, respectively). Following Schmith (1995), the geostrophic wind speed is calculated as

$$w_g = (u_g^2 + v_g^2)^{1/2} \tag{1}$$

with components

$$u_g = -\frac{1}{\rho f}\frac{\partial P}{\partial Y} = -\frac{b}{\rho f} \quad \text{and} \quad v_g = \frac{1}{\rho f}\frac{\partial P}{\partial X} = \frac{a}{\rho f} \tag{2}$$

where $\rho$ is the density of air, $f$ the Coriolis parameter, and $a$ and $b$ represent respectively the zonal and meridional pressure gradients and are calculated by fitting a plane to the three SLP values $P_1$, $P_2$, and $P_3$. Specifically, the three SLP values determine unique constants $a$, $b$, and $c$ in the following set of equations (Schmith 1995):

$$\begin{cases} P_1 = aX_1 + bY_1 + c = aR\lambda_1 \cos\phi_1 + bR\phi_1 + c \\ P_2 = aX_2 + bY_2 + c = aR\lambda_2 \cos\phi_2 + bR\phi_2 + c \\ P_3 = aX_3 + bY_3 + c = aR\lambda_3 \cos\phi_3 + bR\phi_3 + c \end{cases} \tag{3}$$

where $R$ is the radius of the earth, and $\lambda_i$ and $\phi_i$ are the longitude and latitude (in arch degrees) of site $i$ at the time of observation, respectively ($X_i$ and $Y_i$ are the Cartesian coordinates). In this study, we set $\rho = 1.25\text{kg/m}^3$ and $R = 63{,}78{,}100$ m, and used the average of $f$ over the three sites [$f = 2\Omega \sin\phi$ at the latitude $\phi$, where $\Omega = 2\pi/(24 \times 3600)$ is the rotation rate of the earth (in arch degree per second)].

## References


Alexander LV, Tett SFB (2005), Recent observed changes in severe storms over the United Kingdom and Iceland. Geophys Res Lett 32:L13704, doi:10.1029/2005GL022371

Alexandersson H, Schmith T, Iden K, Tuomenvirta H (1998) Long-term variations of the storm climate over NW Europe. Glob Atmos Ocean Syst 6:97–120

Alexandersson H, Tuomenvirta H, Schmith T, Iden K (2000) Trends of storms in NW Europe derived from an updated pressure data set. Clim Res 14:71–73

Bengtsson L, Hodges KI, Roeckner E (2006) Storm tracks and climate change. J Clim 19:3518–3543

Environment Canada (cited 2004) The National Archives System QC program checks for hourly SA's. http://nadm.ontario.int.ec.gc.ca/Intranet/nadm/nas/quality_control/hourlies_e.htm

Gillett NP, Zwiers FW, Weaver AJ, Stott PA (2003) Detection of human influence on sea-level pressure. Nature 422:292–294

Gillett NP, Allan RJ, Ansell TJ (2005) Detection of external influence on sea level pressure with multi-model ensemble. Geophys Res Lett 32:L19714. doi:10.1029/2005GL023640

Gleason, BE, Compo GP, Matsui N, Yin X, Vose RS (2008) The integrated surface pressure databank (ISPD) Version 2.1, National Climatic Data Center, Asheville, NC, pp 1–12. ftp://ftp.ncdc.noaa.gov/pub/ispd/doc/ISPD2_1.pdf

Gulev SK, Zolina O, Grigoriev S (2001) Extratropical cyclone variability in the Northern Hemisphere winter from the NCEP/NCAR reanalysis data. Clim Dyn 17:795–809

Kendall MG (1955) Rank Correlation Methods. Charles Griffin, 196pp

Hess A, Iyer H, Malm W (2001) Linear trend analysis: a comparison of methods. Atmos Environ 35:5211–5222

Hirsch RM, Slack JR (1984) A nonparametric trend test for seasonal data with serial dependence. Water Resour Res 20:727–732

Hirsch RM, Slack JR, Smith RA (1982) Techniques of trend analysis for monthly water quality data. Water Resour Res 18:107–121

Hurrell JW (1995) Decadal trends in the North Atlantic Oscillation: regional temperatures and precipitation. Science 269:676–679

Hurrell JW, van Loon H (1997) Decadal variations in climate associated with the North Atlantic oscillation. Climatic Change 36:301–326

Jung T, Hilmer M, Ruprecht E, Kleppek S, Gulev SK, Zolina O (2003) Characteristics of the recent eastward shift of interannual NAO variability. J Clim 16:3371–3382

Leckebusch GC, Ulbrich U (2004) On the relationship between cyclones and extreme windstorms over Europe under climate change. Glob Planet Change 44:181–193

Leckebusch GC, Koffi B, Ulbrich U, Pinto JG, Spangehl T, Zacharias S (2006) Analysis of frequency and intensity of winter storm events in Europe on synoptic and regional scales from a multi-model perspective. Clim Res 31:59–74

Mann HB (1945) Non-parametric tests against trend. Econometrica 13:245–259

Matulla C, Schoener W, Alexandersson H, von Stroch H, Wang XL (2008) European Storminess: Late nineteenth century to present. Clim Dyn 31:125–130. doi:10.1007/s00382-007-0333-y

McCabe GJ, Clark MP, Serreze MC (2001) Trends in Northern Hemisphere surface cyclone frequency and intensity. J Clim 14:2763–2768

Pinto JG, Ulbrich U, Leckebusch GC, Spangehl T, Reyers M, Zacharias S (2007) Changes in storm track and cyclone activity in three SRES ensemble experiments with the ECHAM5/MPI-OM1 GCM. Clim Dyn 29:195–210

Schmith T (1995) Occurrence of severe winds in Denmark during the past 100 years. In: Proceedings of the sixth international meeting on statistical climatology, pp 83–86

Schmidt H, von Storch H (1993) German Bight storms analyzed. Nature 365:791

Schmith T, Alexandersson H, Iden K, Tuomenvirta H (1997) North Atlantic–European pressure observation 1868–1995 (WASA dataset 1). Technical Report 97-3, Danish Meteorological Institute, Copenhagen, Denmark

Schmith T, Kaas E, Li T-S (1998) Northeast Atlantic winter storminess 1875–1995 re-analyzed. Clim Dyn 14:529–536

Trenberth KE et al (2007) Observations: surface and atmospheric climate change. In: Solomon S et al (eds) Climate change 2007: the physical science basis. Contribution of Working Group I to the Fourth Assessment Report of the Intergovernmental Panel on Climate Change. Cambridge University Press, New York, USA, 944pp

Ulbrich U, Christoph M (1999) A shift of the NAO and increasing storm track activity over Europe due to Anthropogenic Greenhouse Gas Forcing. Clim Dyn 15:551–559

Ulbrich U, Pinto JG, Kupfer H, Leckebusch GC, Spangehl T, Reyers M (2008a) Northern Hemisphere storm tracks in an ensemble of IPCC climate change simulations. J Clim 21:1669–1679

Ulbrich U, Leckebusch GC, Pinto JG (2008b) Extra-tropical cyclones in the present and future climate: a review. Theor App Climatol (accepted)

Uppala SM and co-authors (2005) The ERA-40 re-analysis. Quart J Roy Meteor Soc 131:2961–3012

Wang XL (2008a) Accounting for autocorrelation in detecting mean shifts in climate data series using the penalized maximal *t* or *F* test. J App Meteor Climatol 47:2423–2444. doi:10.1175/2008JAMC1741.1

Wang XL (2008b) Penalized maximal *F* test for detecting undocumented mean shift without trend change. J Atmos Oceanic Technol 25:368–384. doi:10.1175/2007/JTECHA982.1

Wang XL, Feng Y (2007) RHtestV2 User Manual. http://cccma.seos.uvic.ca/ETCCDMI/software.shtm (published online). Climate Research Division, Science and Technology Branch, Environment Canada, Toronto, Ontario, Canada. 19 pp

Wang XLL, Swail VR (2001) Changes of extreme wave heights in Northern Hemisphere Oceans and related atmospheric circulation regimes. J Clim 14:2204–2221

Wang XLL, Swail VR, Zwiers FW (2006a) Climatology and changes of extra-tropical cyclone activity: comparison of ERA-40 with NCEP/NCAR Reanalysis for 1958–2001. J Clim 19:3145–3166. doi:10.1175/JCLI3781.1

Wang XLL, Wan H, Swail VR (2006b) Observed changes in cyclone activity in Canada and their relationships to major circulation regimes. J Climate 19(6):896–915. doi:10.1175/JCLI3664.1

Wang XLL, Swail VR, Zwiers FW, Zhang X, Feng Y (2008) Detection of external influence on trends of atmospheric storminess and northern oceans wave heights. Clim Dyn (in press). doi:10.1007/s00382-008-0442-2

WASA Group (1998) Changing waves and storms in the Northeast Atlantic? Bull Am Meteor Soc 79(5):741–760